Immobilization of ^{129}I in nuclear waste glass matrixes synthesized under high-pressure conditions: an experimental study

Yann Morizet, Jonathan Hamon, Carole La, Valentin Jolivet, Tomo Suzuki-Muresan, Michael Paris

Immobilization of ^{129}I in nuclear waste glass matrixes synthesized under high-pressure conditions: an experimental study

Yann MORIZET[a*], Jonathan HAMON[b], Carole LA[a], Valentin JOLIVET[a,b,c], Tomo SUZUKI-MURESAN[c], Michael PARIS[b]

[a]Université de Nantes, Nantes Atlantique Universités, Laboratoire de Planétologie et Géodynamique de Nantes (LPG), UMR CNRS 6112, 2 rue de la Houssinière, 44322 Nantes Cedex, France

[b]Université de Nantes, CNRS, Institut des Matériaux Jean Rouxel (IMN), 44000 Nantes, France

[c]SUBATECH (IMT Atlantique, CNRS/IN2P3, Université de Nantes), BP 20722, 44307 Nantes Cedex 3, France

*Corresponding author: Yann Morizet

Postal address:

Laboratoire de Planétologie et Géodynamique (LPG), UMR-CNRS 6112, Université de Nantes.

2 rue de la Houssinière, 44322 Nantes Cedex (FRANCE)

phone: +33 (0) 2 5112 5491

fax: +33 (0) 2 5112 5268

*E-mail: yann.morizet@univ-nantes.fr

Abstract

There is a major environmental concern in finding a sustainable solution to immobilize the ^{129}I, a by-product of nuclear industry. The use of aluminoborosilicate glasses represents a good compromise. However, this solution does not appear adequate for ^{129}I owing to its volatility at high-temperature during the vitrification process. In the present work, we use a high-pressure (1.5 GPa) apparatus to synthesize I-rich aluminoborosilicate glasses.

We show that the use of high-pressure conditions enhances the I solubility in glasses by several orders of magnitude as compared to 1 bar synthesis: I solubility up to 5.7 mol.%. We observed that I is more solubilized in Na-rich as compared to Ca-rich glass. Investigation of the I speciation using XPS also reveals that I solubility in glasses is much higher as I dissolves as I^{5+} in comparison to I^-.

Our work shows that using high-pressure appears to be a reliable solution for dissolving a large quantity of I within the structure of aluminoborosilicate glasses for the conditioning of nuclear waste. We also demonstrate that oxidized I waste form should be employed to greatly increase I solubility in nuclear waste glasses. Therefore, it represents a potential pathway for solving the immobilization of ^{129}I produced by anthropic nuclear activity.

Keywords: nuclear waste, ^{129}I radioisotope immobilization, intensive conditions, densified glass

1. Introduction

The radioisotope ^{129}I is a by-product of nuclear reactors and is considered as an intermediate activity nuclear waste owing to its radiotoxicity, its long half-life (15.7 My) and its high mobility in the environment.[1-14] For these reasons, the disposal in geological repository of ^{129}I

requires a chemically stable and durable matrix. There has been a great deal of effort in formulating matrixes able to accommodate a large quantity of iodine (I) in their structure;[15-22] which are stable through time and under natural environmental conditions (i.e. ground water circulation). In the list of potential matrixes, the use of borosilicate glasses is a general adopted solution for nuclear waste immobilization;[23-29] however, it cannot be applied to immobilize I. The standard process to synthesize borosilicate glasses involves melting at high-temperature and ambient pressure. Owing to its high volatility, the borosilicate glass matrix does not retain I sufficiently during the high-temperature process and I escapes in the atmosphere as I_2 gas. Previous studies reported an iodine solubility up to 0.7 mol.% in aluminoborosilicate glasses synthesized at or near ambient pressure.[30-33] More recently, there have been several experimental studies conducted under high-pressure conditions and investigating I solubility in glasses with different applications: either Earth sciences[34,35] or nuclear sciences.[36] Under high-pressure conditions, the I solubility is enhanced in aluminoborosilicate glasses. For instance, Jolivet et al.[36,37] studied the I solubility in the International Simple Glass (ISG)[38] and typical Low Activity Waste glass (LAW)[32,33] synthesized in the pressure range 0.5-2.0 GPa and temperature above 1300°C. They reached a I solubility up to 2.5 mol.% in the typical LAW glass; thus demonstrating that the use of pressure represents a potential adequate solution for immobilizing large quantities of ^{129}I in aluminoborosilicate glass matrixes, therefore reducing the volume of nuclear wastes at geological disposal.

Nonetheless, we have a limited knowledge of the solubility I behavior in aluminoborosilicate glasses because of the lack of available experimental data. The most recent experimental investigations showed that boron content and alkali content play an important role on I solubility: increasing the boron and alkali and alkaline-earth contents induce an increase in I solubility.[36,39,40] However, the effect that other cations in the glass composition induces on I

79 solubility is unknown in detail. By analogy, in the case of CO_2, it has been demonstrated that
80 CO_2 solubility in silicate glasses is affected by the nature of the charge compensating
81 cation.[41,42] Whether I adopts a comparable behavior in aluminoborosilicate glasses is still
82 unknown. Furthermore, the effect of mixed alkaline or alkaline-earth elements on I solubility
83 (i.e. dissolution mechanism) is currently not deciphered. This aspect is crucial to determine
84 because the mixed alkaline or alkaline-earth effect (MAE) is known to affect the glass
85 properties in a complex non-linear behavior.[43-49]

86 Iodine has the particularity to present several redox states: -1 (I^-, iodide), +5 (I^{5+} as IO_3^-, in
87 iodate) and +7 (I^{7+} as IO_4^-, in periodate). Up to now, previous works only studied the I
88 solubility in aluminoborosilicate glasses when I is thought to be dissolved under its reduced
89 form: I^- species. Hence, the effect oxidation conditions induce on I solubility in
90 aluminoborosilicate glasses are unknown. This gap in our understanding of I behavior needs
91 to be fulfilled considering that redox conditions are known to dramatically influence the
92 volatile solubility. For example, sulfur (S) is a volatile element implied in magmatic systems,
93 which exhibits several oxidation states: S^{2-} (sulfide) to S^{6+} (sulfate).[50,51] Experimental data
94 and thermodynamic models showed that S solubility was more important in silicate glasses
95 when S dissolved as S^{6+} (i.e. SO_4^{2-}) species.[52-54]

96 In the present work, we followed an experimental approach to investigate the change in I
97 solubility in aluminoborosilicate glasses synthesized under intensive conditions: 1.5 GPa and
98 1400°C. We focused on glass compositions having various XNa (Na/Na+Ca) values to
99 determine if the nature of the charge compensating cation plays a role on I solubility.
100 Moreover, we investigated the influence of I redox state (I^-, I^{5+} and I^{7+} redox state) on the I
101 solubility. We used spectroscopic methods to determine the iodine speciation in the
102 synthesized glasses. Based on these results, we proposed an I dissolution mechanism as a
103 function of the observed I speciation in glasses. A discussion on the future direction to

formulate a borosilicate glass matrix that is specific for a sustainable immobilization of ^{129}I radioisotopes is also proposed.

2. Materials and methods

2.1. Starting materials and high-pressure synthesis

The investigated aluminoborosilicate glass compositions are reported in Table 1. The starting materials were prepared in the system SiO_2-B_2O_3-Al_2O_3-CaO-Na_2O from a mixture of spec pure oxides (SiO_2, Al_2O_3, B_2O_3 and CaO) and carbonates (Na_2CO_3). In order to determine the effect of varying network modifying cations on I solubility, we prepared the CN starting compositions with varying XNa (Na/Na+Ca) values: C_{35}, XNa = 0; C_{30}, XNa = 0.25; C_{20}, XNa = 0.6; C_{10}, XNa = 0.8; C_0, XNa = 1. It should be pointed out that in the synthesized compositions the exchange between Ca and Na is made based on the oxygen quantity (i.e. x mole CaO is replaced by x mole Na_2O). Hence, the number of mole for Na is twice as much as the Ca mole in the exchange. From the electric charge point of view, the exchange between CaO and Na_2O keeps the positive charges unchanged. Starting powders were carefully grinded in an agate mortar under dry conditions. The adopted methodology involved a two-step synthesis: 1) synthesis of the base glass without iodine at ambient pressure and 2) high-pressure synthesis with iodine using the initial base glass. We prepared the ambient pressure glasses (CN-0 series) by melting and quenching in a platinum crucible the starting powders at 1200°C in a box furnace under fully oxidizing conditions for two hours and quenching in cold water. The composition of the recovered clear glasses was determined prior to high-pressure experiments (see Table 1).

We used the recovered glass powders made at ambient pressure for the high-pressure experiments. Therefore, at a given composition, a comparison between samples of the different series is possible. Any strong departure from the CN-0 glass composition for high-pressure synthesized glass would indicate a possible heterogeneity or partial crystallization.

We synthesized three series of high-pressure I-bearing glasses. The CN-1 glass series is loaded with I_2 as the source of I during the experiments. The CN-2 glass series is loaded with I_2O_5 as the source of I during the experiments. The CN-3 glass series is loaded with I_2O_5 + PtO_2 providing an additional source of O_2 during the experiment. The objective is to determine the impact of different I sources and various oxygen concentrations on the I solubility, speciation, and I dissolution mechanism in aluminoborosilicate glasses. The most prominent difference between the I starting source is the oxygen concentration that is higher in the CN-2 and even higher in CN-3 experimental series in which PtO_2 has been added. During the high-pressure and high-temperature experiments, I_2O_5 dissociates at ~350°C into I_2 and O_2; and in a similar manner, PtO_2 decomposes at 450°C into Pt and O_2.

We used welded shut 5.4 mm outer diameter Pt capsules for the high-pressure high-temperature experiments. We loaded the I source (and PtO_2) at the bottom of the capsule and the glass powder added on top of it. As shown in Table 1, we loaded approximately the same amount of I in every experiment: ~13 mol.% I as I_2 or I_2O_5 calculated from the number of mole of added iodine divided by the total number of mole of oxides in the glass. This amount of I is supposed to be above the saturation;[36] consequently, during the experiments, there is a coexistence between a melt phase and an excess I-rich fluid phase. Considering that the initial amount of I is constant from one experiment to another, the measured I content in the recovered glass corresponds to the actual I solubility (i.e. the maximum I dissolved in the glass matrix at a given composition and given intensive conditions). The amount of added O_2 is reported in Table 1 and is calculated considering the complete dissociation of I_2O_5 and PtO_2. For the CN-2 experiments, the calculated O_2 is ~16 mol.%; for the CN-3 experiments, the calculated O_2 is higher with ~20 mol.% O_2 added coming from the dissociation of both I_2O_5 and PtO_2.

153 The high-pressure experiments have been carried out in end-loaded piston-cylinder apparatus
154 (LPG Nantes). We used ¾ inch talc-Pyrex assembly with the Pt capsule placed inside the
155 graphite furnace and surrounded by MgO-based ceramics for preventing contact between the
156 capsule and the graphite furnace. It should be emphasized that oxygen fugacity conditions
157 were not controlled during the experiments but are intrinsically fixed by the high-pressure
158 talc-Pyrex assembly itself and are relatively oxidizing. We achieved the experimental
159 conditions (1.5 GPa and 1400°C) using the protocol described in previous works.[55] We
160 applied a pressure of 1 GPa followed by heating to 500°C and left for 5 min for high-pressure
161 assembly relaxation. We then increased the pressure up to 1.5 GPa. We added a 10%
162 correction on the pressure owing to the friction in the talc-Pyrex assembly.[56] At 1.5 GPa, the
163 pressure is controlled automatically by a Stigma© needle pump preventing the pressure
164 variation during the experiment. The temperature was increased automatically up to 1400°C
165 at a rate of 50°C/min. During the experiment, the temperature was controlled by a B-type
166 ($PtRh_6$-$PtRh_{30}$) thermocouple located at the top of the capsule and accurate to ±1°C. The run
167 duration was set to 4h for all the experiments to be reproducible. We stopped the experiment
168 by cutting-off the power and quench rate is estimated at ~100°C/sec. in the first 500°C. We
169 performed an isobaric quench to avoid the presence of bubbles in the obtained glass. The
170 recovered capsule was weighed for eliminating any possible leakage and I loss during the
171 experiment. The collected sample consists in a glass tainted in brown and covered at the
172 surroundings and along the experimental charge by a dark residue corresponding to the I
173 excess present during the experiments. Under high-pressure and high-temperature conditions,
174 I is in the fluid state but in a solid state at ambient conditions. The I residue is present across
175 the whole length of the sample suggesting that under run conditions I is distributed throughout
176 the melt. This residue was totally removed by washing in ethanol. Optical examination did not
177 reveal the presence of crystalline phases in the glass; however, for one particular sample

178 (C_0N_{35}-2) we suspect the presence of NaI nanocrystals, however, these crystals are not
179 observed during Scanning Electron Microscopy Energy Dispersive Spectroscopy analysis. A
180 dark residue was present at the bottom of the capsule for CN-3 experiments, corresponding to
181 the Pt coming from the dissociation of PtO_2.

182 **2.2. Scanning Electron Microscopy Energy Dispersive Spectroscopy**

183 The major element and iodine concentrations were obtained with a JEOL JSM 5800LV
184 Scanning Electron Microscope, equipped with a SDD SAMx dispersive spectrometer (SEM
185 EDS, IMN Jean Rouxel Nantes). The analytical conditions were 15 kV for voltage and 0.5 nA
186 for current. The current beam was regularly controlled during all analytical campaigns to
187 ensure a reproducible electron flow. We mounted the CN glass chips in epoxy plugs and each
188 plug includes an ISG glass chip considered as a standard glass to our SEM
189 measurements.[36,38,57] The ISG standard glass was analyzed prior and after the CN glass chips
190 analyses to check for possible instrumental drift. The acquisitions were conducted on a 20 µm
191 spot size to avoid alkali (Na) loss under the electron beam. We performed 10 scans of 1 min.
192 for each sample as a peak threshold criterion to reduce the minimum acceptable concentration
193 for identification. We used internal standards for the elements quantification: LaB_6 for B_2O_3,
194 corundum for Al_2O_3, wollastonite for SiO_2 and CaO, NaCl for Na_2O, and RbI for I. In most of
195 the case, the B_2O_3 is lower than the expected B_2O_3 (~30 mol.%, see Table 1). With all
196 precautions during SEM EDS analyses, we obtain an uncertainty on element (including
197 iodine) measurements that is typically ±0.2 mol.%.

198 **2.3. Laser Ablation-Inductively Coupled Plasma-Mass Spectrometry**

199 Glass I content was also determined using a Laser Ablation-Inductively Coupled Plasma-
200 Mass Spectrometry (LA-ICP-MS, LPG Nantes) for providing more robust results on the I
201 solubility. The spectrometer is an ArF excimer laser (193 nm, Analyte G2, Photon Machines)

202 that is coupled to a quadrupole ICP-MS (Varian Bruker 820-MS). The ablations were
203 performed in a HelEx II 2-Volume Cell with He as carrier gas. We used a laser energy density
204 of 4.54 J.cm^{-2} and with a repetition rate of 10 Hz. All the analyses were performed in a spot
205 mode with circular spots size of 110 µm in diameter. At least five acquisitions were collected
206 on each I-bearing glass sample. Acquisition time was set to 30 s. with points collected every
207 ~0.25 s. (total number of point per analysis = ~120), preceded and followed by a 30 s. blank
208 acquisition. The washout time of the ablation cell was approximately 50 s., due to the long
209 remanence of iodine in the system. With this analytical setup, the pit size is estimated to ~20
210 µm in depth.

211 The data were calibrated against several glass samples. The recorded isotopes were ^{127}I and
212 ^{27}Al and this latter one was used as an internal standard. We calibrated the I content with two
213 high-pressure ISG glasses doped with I (1.29 and 1.34 mol.% I) and with known Al_2O_3
214 content of 4.08 and 4.02 mol.%, respectively. Both I and Al_2O_3 contents have been quantified
215 using Electron Probe Micro-Analyses (EPMA, ISTO Orléans). The good agreement between
216 EPMA and LA-ICP-MS collected data are provided in Suppl. Mat. and indicates that LA-ICP-
217 MS is a reliable technique for the quantification of our elemental concentrations in I-bearing
218 borosilicate glasses.

219 **2.4. X-ray Photoelectron Spectroscopy**

220 We used X-Ray Photoelectron Spectroscopy (XPS) to determine the I speciation in our high-
221 pressure borosilicate glasses. Several crystalline standards (NaI, $NaIO_3$ and CaI_2O_6) were also
222 analyzed for fingerprinting the I speciation in glasses.

223 We acquired the XPS spectra on Kratos Axis Ultra and Nova spectrometers (IMN Jean
224 Rouxel) equipped with a monochromatic Al Kα radiation operating at 1486.6 eV and 300 W.
225 The glass chips (~3x3 mm^2) showing a surface from the bulk of the experimental charge were

loaded into the sample chamber and at high vacuum (<8 10^{-8} mbar). The beam size on the sample was 300x700 μm^2. We acquired the spectra with different pass energy: at 160 eV for the wide spectrum with a step of 0.5 eV and at 20 eV for high-resolution XPS spectra on elements with a step of 0.1 eV. We referenced the spectra against the adventitious C 1s transition at 284.8 eV.[58,59] We used cycling acquisitions (10 to 15 cycles) to determine if the sample spectra are changing under the X-ray beam. In the case that no change is observed between the cycles, the final spectrum is obtained by averaging the sum of spectra obtained. Currently, this was the case for CN-1 and CN-2 glass series. On the contrary, for CN-3 glass series we observed that after the first cycle the I XPS spectrum was strongly affected by the X-ray beam energy. We also performed XPS acquisitions on several glass chips for a given sample charge to assert the homogeneity of the I speciation.

For I species, the high resolution XPS spectra were acquired at the I 3d ~620 eV core level. The spectral window was set between 608 and 643 eV to be sufficiently large for background subtraction. The obtained I 3d XPS spectra were treated with CasaXPS© software. We used a Tougaard function for background subtraction.[60] The I 3d spectra were fitted with asymmetric Gaussian-Lorentzian lines and only the I $3d_{5/2}$ peak was considered. The I $3d_{5/2}$ peak exhibits higher intensity than the one for the I $3d_{3/2}$.[61]

3. Results

3.1. I content and distribution in glasses from LA-ICP-MS and SEM EDS

Figure 1 shows the I content determined by LA-ICP-MS as a function of the I content obtained by SEM EDS. From the general viewpoint, we observe that both I contents obtained with LA-ICP-MS and SEM EDS provide comparable and consistent results. However, it appears that LA-ICP-MS results are systematically higher than SEM EDS for the samples with the highest I content. As mentioned earlier, the error bar on the I content determined by SEM EDS is on the order of ±0.2 mol.%. The error bars on the I content determined by LA-

ICP-MS determined from the standard deviation of replicated measurements and is within the point except for C_0N_{35}-2 (±0.6 mol.%).

For the remaining of the manuscript, we will preferentially refer to the I content determined by LA-ICP-MS. First, the error on the I content is much smaller from LA-ICP-MS than from SEM EDS. Second, the LA-ICP-MS analyzed glass volume (~110x20 μm^3) is much more important than for SEM EDS (~20x1 μm^3), therefore, we consider that the reported LA-ICP-MS I content is more representative of the I bulk content. Although, a slight deviation from the true I content in glasses is still possible using LA-ICP-MS results considering that the calibration curve is obtained with two standard glasses with 1.29 and 1.34 mol.% I that is lower than the I content measured in CN glasses (up to 5.7 mol.%). However, the possible deviation will be lower than the one associated with SEM EDS measurements for which RbI (50 mol.% I) is used as a standard.

For $C_{20}N_{15}$-22, we have investigated the I concentration in detail using LA-ICP-MS. I concentration profiles were obtained through the entire Pt capsule length and width (see Figure 2). We acquired several transversal profiles using the laser ablation point mode and 48 points were acquired (the entire set of data is provided in Suppl. Mat.). The results are shown in Figure 2 as a contour plot for I. The lines of equal contents have been drawn from linear extrapolation. We observe that the I concentration is almost entirely homogeneous throughout the sample charge. These measurements provide the typical error on the I solubility after high-pressure experiments. For this sample, the I content ranges from 4.5 to 4.8 mol.%. Based on the 48 points, we obtain an average value of 4.6 mol.% I with a standard deviation of 0.1 mol.%. This error is taken as representative of the I solubility error for the whole set of samples.

3.2. I solubility in glasses

The measured I solubility in mol.% is reported in Table 1 along with the major element composition measured for each glass. We plotted the I solubility as a function of XNa (Na/Na+Ca in mol.%) in Figure 3. We fitted each I solubility glass series with a polynomial function. For the synthesized high-pressure glasses, the measured I solubility ranges from 0.5 to 5.7 mol.%. Three striking features are observed in Figure 3: 1) the highest I solubility is observed for CN-2 glasses loaded with I_2O_5 as the I initial source; 2) the I solubility change is non-linear with respect to the XNa change, regardless of the I source; and 3) the higher loaded O_2 does not lead to the highest I solubility (i.e. lower I solubility in CN-3 than in CN-2 glasses).

In Figure 3, the higher I solubility in the CN-2 glasses as compared to CN-1 and CN-3 ones is clearly observed for all glass compositions except $C_{35}N_0$-2. In $C_{30}N_5$, the difference in I solubility is 1.5 mol.% (0.5 to 2.0 mol.% for $C_{30}N_5$-1 and $C_{30}N_5$-2, respectively). Such difference in I solubility is well above any possible error on the I measurement using LA-ICP-MS. For $C_{20}N_{15}$, the difference in I solubility is even larger: 4.3 mol.%. For the $C_{35}N_0$ glass composition, the I solubility is comparable regardless of the initial I source or added O_2: 1.2 and 1.3 mol.% for $C_{35}N_0$-1 and $C_{35}N_0$-2, respectively. The Ca-free C_0N_{35} glasses exhibit the highest I solubility with 3.9 and 5.7 mol.% for C_0N_{35}-11 and C_0N_{35}-2, respectively. Globally, increasing the XNa in the glass composition induces an increase in I solubility. In fact, Ca-rich glasses are not as favorable for dissolving large quantities of I as Na-rich glasses. Based on X-ray Absorption Spectroscopic results, previous studies also suggested a strong affinity between iodine and sodium.[31-33,62]

For the CN-1 glasses, we observe in Figure 3 a clear parabolic evolution of the I solubility as a function of XNa. The I solubility is decreasing from 1.2 to 0.5 mol.% between $C_{35}N_0$-1 and $C_{30}N_5$-1 and $C_{20}N_{15}$-1, increases to 1.7 mol.% for $C_{10}N_{25}$-1 and further increases to more than 3 mol.% I in C_0N_{35}. The non-linear change in I solubility in the CN-1 glasses as a function of

XNa is currently unexplained. We suspect that there is a strong intermixing between Na and Ca cations in the glass structure that could explain the I solubility behavior. It is comparable to the mixed alkali/alkaline-earth effect identified in glasses and inducing non-linear evolution of the glass physical properties.[48,49,63,64]

In CN-2, the I solubility behavior is not the same and does not show a parabolic evolution but a sub-linear trend is observed and shows an increasing I solubility from $C_{35}N_0$-2 at 1.3 mol.% to C_0N_{35}-2 at 5.7 mol.%. It should be stressed that both the non-linearity (for instance in CN-1 glasses) of I solubility and the impact of the iodine source on the I solubility were not anticipated; demonstrating that I has a complex behavior in aluminoborosilicate matrix. On the contrary to CN-1 glasses, the Ca/Na intermixing does not seem to induce a negative effect on I solubility, which is interpreted as resulting from the increasing oxygen concentration within the glass in CN-2. The increase in oxygen concentration might induce a larger dispersion of positive cation charges for compensation and therefore allowing more space for I to be accommodated. Furthermore, Cormier and Cuello[65] showed that an increase in cation coordination (due to the increase in oxygen concentration in the case of CN-2 glass series) is accompanied by an increase in bond length; hence, facilitating the I accommodation in the glass. It also implies that the I local environments in CN-2 glass series is not affected by the Ca/Na intermixing and I environments are charge compensated by Ca and Na without distinction.

Except for $C_{35}N_0$, the solubility results for CN-3 glass series appear intermediate between I solubility for CN-1 and CN-2. For $C_{35}N_0$-33, the measured I solubility (1.3 mol.%) is on the same order as for $C_{35}N_0$-1 and $C_{35}N_0$-2. It suggests that regardless of the I form the I solubility is not strongly affected in pure calcic glass composition; on the contrary to mixed Na-Ca glass compositions in which the nature of I source plays a major role on I solubility. The intermediate value for I solubility in CN-3 glass series was not expected (i.e. higher I

325 solubility was expected considering the higher O_2 concentration) and is currently not clearly
326 explained and additional experimental work is required for investigating further this aspect.

327 **3.3. I speciation in glasses**

328 **3.3.1. General case**

329 The Figure 4 shows several I $3d_{5/2}$ XPS spectra obtained for $C_{35}N_0$ and C_0N_{35} glass
330 compositions and for the two initial source of iodine: either I_2 (Figure 4A and C) or I_2O_5
331 (Figure 4B and D). The spectra are shown with the same range of energy between 610 and
332 630 eV. The entire set of obtained XPS spectra along with the corresponding simulation is
333 provided in the Suppl. Mat.. The spectra in Figure 4 are also presented with the subsequent
334 deconvolution and the corresponding I speciation.

335 For $C_{35}N_0$, we observe two different I speciation depending on the initial I source in the
336 starting material. In $C_{35}N_0$-1 (I_2 loaded, Figure 4A), we observe a peak at ~619 eV and a small
337 shoulder at ~621 eV. In $C_{35}N_0$-2 (I_2O_5 loaded, Figure 4B), the XPS spectrum exhibits two
338 major contributions: one at ~619 eV and one at ~624.5 eV. The peak at 619 eV can be
339 assigned to I^- species,[61,66,67] the peak at 621 eV can be assigned to I^0 species,[68] and the peak at
340 624.5 eV can be assigned to I^{5+}.[68,69] In $C_{35}N_0$-1, when I_2 is loaded in the starting material,
341 iodine is mostly dissolved as I^- species (93.9%), and a small proportion of I^0 is also identified
342 (6.1%). It implies that for a total of 1.2 mol.% I, I^- represents 1.13 mol.% and I^0 represents
343 0.07 mol.% (see Table 1). In $C_{35}N_0$-2, the deconvolution of the XPS spectrum is more
344 complex as the peak at ~619 eV cannot be decomposed with a single asymmetric line and a
345 small contribution at ~621 eV is requested to reproduce the entire spectrum of the I $3d_{5/2}$.
346 Nevertheless, when I_2O_5 is loaded in the starting material, iodine is mostly dissolved as I^{5+}
347 (58.6%) with a non-negligible contribution of I^- (28.8%) and a small contribution of I^0
348 (12.7%). With a measured I solubility of 1.3 mol.%, I^{5+} represents 0.76 mol.%, I^- represents
349 0.37 mol.% and I^0 represents 0.17 mol.%. As shown in Table 1, the other glass samples

exhibit the same behavior: when I_2 is loaded, the I speciation in the glass is mostly I^- and accompanied by a small quantity of I^0; when I_2O_5 is loaded, the I speciation in the glass is a mixture of I^{5+}, I^0 and I^-. Combined with the I solubility results, we observe that the maximum I solubility is obtained when I is dissolved mostly as I^{5+}.

The XPS results obtained on the C_0N_{35}-11 glass sample are comparable to the results obtained for $C_{35}N_0$-1 with I^- as the dominant dissolved I species (Figure 4C): 96% I^- and 4% I^{5+}. For this sample, we obtain an I solubility of 3.9 mol.%. The XPS spectrum for C_0N_{35}-2 shows the predominance of I^{5+} as the I dissolved species, hence comparable to the results obtained on the other glasses (see Table 1). For C_0N_{35}-2, the I solubility is 5.7 mol.%. For the whole glass compositions, we observe that I solubility is positively correlated to the increase in I^{5+}.

For $C_{35}N_0$-2 sample, several XPS spectra were recorded on different glass chips collected from the experimental charge with the objective to determine if the I speciation is homogeneous within the experimental charge. Four glass chips from $C_{35}N_0$-2 were collected along the experimental charge (from top to bottom) and analyzed by XPS for investigating the homogeneity of the I speciation. The results are shown in Figure 5 with an estimated error bar of 10% in relative to the data. The I speciation is slightly heterogeneous: I^- ranges from 20 to 32%; I^{5+} ranges from 58 to 74%; I^0 is roughly constant from 5 to 9%. We obtain the following average values and standard deviation: $I^- = 26.1 \pm 8.4\%$, $I^{5+} = 66.5 \pm 8.0$, and $I^0 = 7.4 \pm 2.9\%$. Therefore, we suggest that the I speciation in CN-2 glasses is accurate to only ±10% in absolute value. This problem does not apply to CN-1 glass series as I^{5+} species are not observed (although 4% I^{5+} is determined for C_0N_{35}-11) from XPS measurements (see Table 1). We explain the strong difference in I speciation between the CN-1 and CN-2 glasses by the different experimental conditions: I_2 loaded in CN-1 and I_2O_5 loaded in CN-2.

3.3.2. Higher oxidation case: $C_{35}N_0$-33 glass

The CN-3 glass series represent a peculiar approach aimed to increase the oxidation conditions prevailing during high-pressure experiments. We choose to increase fO_2 conditions by doping the sample with PtO_2 that decomposes into Pt and O_2 at high-temperature. The expected result was an increase in I solubility, however, as shown in Figure 3 we do not observe such an increase: I solubility slightly decreases in CN-3 glasses. During XPS analyses, we have observed that I speciation was highly unstable under X-ray beam. We show in Figure 6 XPS spectra obtained on $C_{35}N_0$-33. Spectra are shown for several successive cycles (Cycle 1, 4 and 9 out of 15) obtained on this glass sample. For the first time, we clearly demonstrate the presence of periodate species with +7 oxidation state with a peak located at ~626 eV.[68,70] The I^{7+} is present along with I^{5+}, I^0 and I^- in this glass sample. This result provides the first evidence for the presence of I^{7+} dissolved in aluminoborosilicate glasses synthesized under high-pressure conditions.

The simulation of the XPS spectrum for $C_{35}N_0$-33 suggests that I^{7+} is present in non-negligible quantity. In Cycle 1, I^{7+} species represent almost one third of the I dissolved species. However, it appears that such highly oxidized species is not stable under the X-ray beam during the successive XPS cycles. As shown in Figure 6, I^{7+} decreases significantly in Cycle 4 and becomes negligible in Cycle 9. The change in the I species proportions for this sample are reported in Figure 7 (data are provided in Suppl. Mat.). We clearly see that I^{7+} quickly destabilizes after 4 analysis cycles and after 15 cycles the I^{7+} totally disappears. On the contrary, we see that the proportion of I^{5+} increases conjointly with the decrease in I^{7+} (I^0 and I^- remain constant) suggesting that there is a conversion of I^{7+} to I^{5+} resulting from the energy of the X-ray beam. We do not observe any increase in the I^0 and I^-. Although, the statistic is not ideal (i.e. proportions obtained on each cycle), we suggest that the I speciation measured at the first cycle represents the true I speciation prevailing in the $C_{35}N_0$-33 glass and derived proportions after Cycle 1 are reported in Table 1. For the $C_{20}N_{15}$-3 and $C_{10}N_{25}$-3, the

399 periodate species is not observed (see Table 1); however, we cannot exclude its presence
400 during the experiment under high-temperature and high-pressure conditions.

401 Above the fact that periodate species appear highly unstable during analytical characterization
402 by XPS, our results also imply that iodate species are probably the most stable oxidized iodine
403 species (see Figure 7). Therefore, a protocol that focuses on increasing further the oxidation
404 conditions might not be efficient in 1) dissolving more iodine and 2) dissolving iodine in its
405 most stable form.

406 ## 4. Discussion

407 ### 4.1. Iodine speciation and dissolution mechanisms: the influence of the redox state

408 In Figure 3, we show that the I loaded form has a dramatic impact on the I solubility and we
409 demonstrate that the change in I solubility is related to the change in I speciation as measured
410 by XPS (see Figure 4). As I^{5+} increases into the glass, there is an increase in I solubility. We
411 have plotted in Figure 8 the change in I solubility as a function of the Overall I Redox State
412 (ORS) calculated from the I speciation in Table 1 with the following equation:

413 $$-1 \times XI^{-} + 5 \times XI^{5+} + 7 \times XI^{7+} = Overall\ I\ redox\ state\ (ORS) \qquad (1)$$

414 In Figure 8, we can observe that there is a positive correlation between I solubility and ORS.
415 This positive correlation is clear for most of the glass compositions. For $C_{20}N_{15}$ the trend is
416 less clear whether the increase is linear or not. For $C_{35}N_0$ glass composition, I solubility does
417 not vary with increasing ORS.

418 The present work represents the first evidence showing that, at constant glass composition and
419 constant intensive conditions, the I solubility depends on the I speciation. At high-pressure
420 and high-temperature, I_2 is under supercritical conditions, which implies that the
421 thermodynamic activity of the I_2^{fluid} equals the thermodynamic activity of the I_2^{melt}. Within the
422 melt iodine atoms ionizes in the surroundings of sodium or calcium to form Na..I or Ca..I

linkages. In the case iodide is only present (i.e. CN-1), we propose the following general chemical reaction for iodide dissolution mechanism:

$$\frac{n}{2} I_2^{melt/fluid} + M^{n+}..O_n^{-\,NBO} \leftrightarrow M^{n+}..I_n^{-} + \frac{n}{2} O_2^{fluid/melt} + \frac{n}{2} O^{BO} \qquad (2)$$

In Eq. 2, M^{n+} is a charge compensating cation for I^- species either Na^+ or Ca^{2+} forming Na..I and Ca..I species.[36,62] In Eq. 2 the I dissolution is accompanied by a rearrangement of the glass network: a Non-Bridging Oxygen (NBO) is transformed into a Bridging Oxygen (BO) implying that I dissolution has a polymerizing effect on the glass structure. However, it is probably a little more complicated than currently mentioned, as the oxygens involved in Eq. 2 might indeed be NBOs from the boron or silicate units. For instance, Jolivet et al.[36] showed that the proportion of BO_4 units (i.e. N4) in the glass is affected by the I dissolution. BO_4 concentration can increase or decrease depending on the glass chemical composition. In Eq. 2, accompanying the polymerization of the network is the production of $1/2O_2$ that is released in the fluid phase. By analogy to the I dissolution as IO_3^- that is enhanced in the case an excess O_2 is present (i.e. CN-2 and CN-3), the release of O_2 in the fluid should induce the dissolution of a limited proportion of IO_3^-. Clearly, it is not the case as the I speciation is mostly I^- (only C_0N_{35}-11 exhibits the presence of IO_3^-, see Table 1).

Under intensive conditions, the oxygen activity is expressed by the oxygen fugacity (fO_2). During the high-pressure experiments, using talc-Pyrex assemblies, the fO_2 has been estimated to be close to QFM+1 in relative to the solid oxygen buffer Quartz-Fayalite-Magnetite.[71,72] These conditions are relatively oxidizing. For instance, in C- and S-bearing high-pressure systems, the oxidized CO_2 and SO_2 (or SO_3) are the dominant species in both the fluid phase and the melt phase.[55,73] However, in the I-bearing system currently studied, I_2 is the dominant species in the fluid phase and Eq. 2 is also controlled by I fugacity (fI_2). To our knowledge, there is currently no available Equation-Of-State for I_2 in the fluid phase

under temperature and pressure conditions preventing from calculating the I_2 thermodynamic activity in the fluid phase under intensive conditions.

In the case of CN-2 glass series, we observe the coexistence between I^- and I^{5+} species, which means that another oxidation/reduction mechanism has to be proposed for constraining the fO_2 conditions. The fact that I^{5+} is observed in the glass implies necessarily that there is an increase in the fO_2 (fO_2 > QFM+1). We used the following chemical reactions for explaining the oxidation/reduction mechanisms and the coexistence of both I^- and I^{5+} species in the CN-2 glasses:

$$I_2 + 2e^- \overset{E_1^0}{\leftrightarrow} 2I^- \qquad (3)$$

$$I_2 + 3O_2 + 2e^- \overset{E_2^0}{\leftrightarrow} 2IO_3^- \qquad (4)$$

The standard potentials for these two reactions are E^0_1 = +0.54 V and E^0_2 = +1.8 V. It follows the global equilibrium reaction:

$$2IO_3^- \overset{K}{\leftrightarrow} 2I^- + 3O_2 \quad (5)$$

With:

$$K = \frac{[I^-]^2 \times f_{O_2}^3}{[IO_3^-]^2} \quad (6)$$

We combined the Nernst and the Gibbs-Duhem equations to determine the K value at 1400°C: 2.56×10^{-8}. Using the I^- and IO_3^- concentrations determined for CN-2 glasses in Table 1, we were able to estimate the fO_2 conditions prevailing during the oxidized experiments with I_2O_5. We obtain a fO_2 on the order QFM+3 (the detailed calculation is provided in Suppl. Mat.), which is consistent with the higher oxidizing conditions imposed by the dissociation of I_2O_5 into I_2 and O_2 during the experiment. The QFM+3 only represents an estimate of the fO_2

condition; a more convenient approach would require the use of solid oxygen buffers during the experiments.

With regards to the actual I dissolution mechanisms within the glass structure, the global equation proposed by Riley et al.[32] involves the coexistence of I^- and I^{5+} species to the proportions of 5:1; however, it cannot apply to our study as the proportion of I^{5+} in CN-2 glasses is well above this ratio (see Table 1). We propose the following equation (Eq. 7) describing the dissolution of I^{5+} species:

$$\frac{n}{2} I_2^{fluid/melt} + \frac{5n}{2} O_2^{fluid/melt} + M^{n+}..O_n^{-\,NBO} \leftrightarrow M^{n+}..(IO_3^-)_n + \frac{n}{2} O^{BO} \quad (7)$$

In Eq. 7, O_2 from the fluid phase (from the dissociation of I_2O_5) and oxygen from the melt ($O^{-\,NBO}$) are used to form iodate species (IO_3^-) with surrounding charge compensating cation M^{n+} either Na^+ or Ca^{2+} forming $Na^+(IO_3^-)$ or $Ca^{2+}(IO_3^-)_2$ units dissolved in the glass. Eq. 7 also implies that the dissolution of I as IO_3^- is favored by an increase in fO_2 during the experiment. This implication is only true to a certain extent considering that we do not observe an increase in the proportion of the IO_3^- proportion in the CN-3 glass series. In a similar way to Eq. 2, the I dissolution as IO_3^- induces a rearrangement of the glass network by consumption of NBOs that change to BOs as a result of the charge compensation by the cation, either Na^+ or Ca^{2+}.

4.2. Consistency between measured I speciation and dissolution mechanisms

Although I dissolved as I^- in glasses equilibrated with pure I_2 is consistent with previous works,[36] it is surprising not to observe IO_3^- coexisting with I^- considering that O_2 is produced during I dissolution (see Eq. 2). Similarly, the mixed IO_3^-/I^- speciation in glasses equilibrated with pure I_2O_5 is questioning, as the quantity of oxygen brought by the dissociation of I_2O_5 should be enough to promote the I dissolution as IO_3^- only (see Eq. 7). We have done the mass balance on oxygen consumed and produced during I dissolution as I^- and IO_3^- as observed in the CN-2 and CN-3 glass series. For the sake of clarity, we have considered that

sodium is the charge balancing cation (i.e. considering calcium as balance element gives the same results).

$$i\,I_2 + c\,Na^{+}..O^{-\,NBO^{total}} + \frac{5}{2}i\,O_2 \rightarrow x\,NaI + y\,Na(IO_3) + (c-x-y)Na^{+}..O^{-\,NBO^{rest}} + O_2^{fluid} \quad (8)$$

With the following number of mole:

$$i + c + \frac{5}{2}i \rightarrow x + y + (c-x-y) + \left(\frac{5}{2}i + \frac{x+y}{2} - \frac{3}{2}y\right) \quad (9)$$

In Eq. 9, the $\frac{x+y}{2}$ on the right-hand side for O_2^{fluid} corresponds to the number of mole produced by the transformation of O^{NBO} to O^{BO} for example with the following equation:

$$2X{-}O^{NBO}..2Na + I_2 \rightarrow 2NaI + X - O^{BO} - X + \frac{1}{2}O_2 \quad (10)$$

In which *X* stands for a network former cation such as Si or B. The $x + y$ is also equal to the dissolved iodine number of mole, *2i.* In Eq. 9, the $\frac{5}{2}i$ quantity corresponds to the number of mole coming from the I_2O_5 dissociation, and the $-\frac{3}{2}y$ quantity corresponds to the consumption of O_2^{fluid} to form iodate. Therefore, the net proportion of O_2 produced in the fluid on the right-hand side of Eq. 9 is $\left(\frac{7}{2}i - \frac{3y}{2}\right)$. The I dissolution implies necessarily that $\left(\frac{7}{2}i - \frac{3y}{2}\right)$ is either equal to 0 or positive. It follows that $3y \leq 7i$. Therefore, we can extract the proportion of iodate formed $\frac{y}{2i} \leq \frac{7}{6}$. Assuming this mass balance on the oxygen, it implies that the upper limit for IO_3^- concentration is 100% in the case I_2O_5 is added to the system. The same calculation can be conducted for the I_2 loaded during the experiment. In such case, the $\frac{5}{2}i$ is removed from the calculation and the upper limit to the proportion of iodate becomes $\frac{y}{2i} \leq \frac{1}{3}$, which corresponds to 33% of IO_3^- formed.

As shown in Table 1, under no circumstances those upper limits are achieved: there is no IO_3^- in the CN-1 glass series and IO_3^- reaches a maximum of 85% in $C_{30}N_5$-2. Consequently, the oxygen availability appears not to be the limiting factor for the formation of IO_3^- species and other controlling parameters (e.g. thermodynamic) are involved in the equilibrated speciation that we actually measure.

4.3. Exploring leads for future ^{129}I immobilization in aluminoborosilicate glasses

^{129}I radioisotope represents a serious environmental problem that requires specific matrixes for immobilization. One goal to our approach is to provide highlights for guiding future research in the elaboration of matrixes for the geological disposal of ^{129}I. However, we are perfectly aware that the synthesized glasses in the present work are essentially designed to obtain the fundamental understanding of the role of Ca and Na on the iodine dissolution in glasses. For instance, the investigated pressure (1.5 GPa) is high in comparison to an industrial process using Hot-Isostatic Press[19,39,40] and the chemical durability of the presently investigated glass compositions remains to be asserted.[74] Considering the lack of experimental data on I solubility, it appears presumptuous to build a reliable model that can be used for predicting I solubility for a wide range of aluminoborosilicate glass compositions. Nonetheless, we can provide a series of preconisation for a future permanent immobilization of ^{129}I radioisotopes.

In Figures 3 and 8, we show that C_0N_{35} glass composition represents the best candidate to dissolve efficiently ^{129}I nuclear waste providing that high oxidation state is imposed during the experiments and I is dissolved in the glass as iodates species. It should be emphasized that the iodate species are the most advantageous form of I with respect to environment as its mobility in clays is lower than the iodide species.[75,76] We suggest that the increase in I solubility with increasing I oxidation state is resulting from the availability of oxygen atoms within the melt to form IO_3^- units. Interestingly, increasing strongly the oxygen concentration

tends to promote the formation of periodate; however, as shown in Figure 7, this species lacks stability within the glass under the XPS beam. This lower stability is likely due to the higher oxygen coordination environment around I^{7+}.[77] Although the periodate stability under natural environmental conditions should be investigated, we suggest that exceedingly high oxidative conditions should be avoided to prevent the formation of periodate species. Meanwhile, sufficiently high oxidation conditions should be maintained to maximize the I solubility. Solid sorbents such as crystalline $NaIO_3$ could be used to ensure high I load and high oxidation conditions during the vitrification process. Moreover, this methodology would increase the Na content in the matrix composition and consequently increasing I solubility due to the higher I affinity for Na-rich glass compositions.

Further experimental work has to be conducted in order to decipher the I solubility change in aluminoborosilicate glasses considering the large range of chemical compositions for nuclear waste glasses.[25,78] For instance, the rationale for I solubility as a function of the nature of the charge compensating cations is not clearly determined. In the present work, we clearly show that I dissolution is favored in Na-rich compositions as compared to Ca-rich compositions. Both cations are close in size but with different charges and different roles within the glass structure. Na^+ is known to act as a charge compensating cation to BO_4 units and AlO_4 units;[79-83] whereas Ca^{2+} acts as a network modifying cation inducing the depolymerization of the glass network.[84-85] As a result, Na^+ is located in the surroundings of weakly charged oxygen atoms (i.e. bridging oxygen, BO), whereas Ca^{2+} is surrounded by highly charged oxygen atoms (i.e. non-bridging oxygen, NBO). However, the nature of oxygen atoms surrounding Na^+ and Ca^{2+} is mitigated considering the mixed alkali effect.[45] Na^+ has more affinity with I^- or IO_3^- species than Ca^{2+}, which can be explained by the weaker nature of the $Na\text{-}O^{BO}$ bonds in the structure compared to $Ca\text{-}O^{NBO}$ bonds. In the case of pure Ca glass composition, Ca^{2+} adopt both roles: charge compensating and network modifying; and I dissolution in that case is still possible (I

562 solubility different from 0) but to a limited extent. As a result, it could be pertinent to
563 investigate the change in I solubility as a function of the size and charge of the non-network
564 forming cations (i.e. Li^+, K^+, Rb^+, Sr^{2+}, Ba^{2+}).

565 **5. Conclusions**

566 Better understanding of the I behavior in borosilicate glasses is a prerequisite for the
567 formulation of future matrixes able to immobilize ^{129}I in geological repositories. In the present
568 work, we have investigated the change in I solubility in a series of borosilicate glass 1) held
569 under high-pressure conditions (1.5 GPa), 2) with varying Ca/Na ratios, and 3) with different
570 sources of I and oxygen to study the effect of redox conditions.

571 We have demonstrated that I solubility is strongly enhanced when the iodine source is I_2O_5
572 instead of I_2. Under highly oxidizing conditions, XPS measurements revealed that iodine is
573 essentially dissolved as I^{5+} species. Increasing further the oxidizing conditions is
574 counterproductive as it implies the presence of the unstable I^{7+} species and does not lead to an
575 increase in I solubility.

576 Regardless of the I speciation, we have shown that there is a non-linear behavior of I
577 solubility as a function of XNa value. Globally, we show I solubility is favored in Na-rich
578 glass compositions, in agreement with previous experimental investigations.

579

580 *Acknowledgements*

581 *The authors are grateful to the Agence Nationale de la Recherche and Région Pays de la*
582 *Loire, which financed the current work through the ANR project "Iodine-CLEAN-UP" (ANR-*
583 *20-CE08-0018) and the Pari Scientifique "CIPress". The authors thank the Laboratoire de*
584 *Planétologie et Géodynamique, the Institut des Matériaux Jean Rouxel, the University of*

Nantes and the CNRS for providing access to the analytical facilities. The authors thank Nicolas Stephant for its support on the SEM/EDS analytical platform. We would like to thank Ida Di Carlo (ISTO) for providing the EPMA analyses.

Reference

1 R. Fuge and C. C. Johnson, *Env. Geochem. Health*, 1986, **8**, 31-54.

2 P. J. Coughtrey, D. J. Jackson and M. C. Thorne, Netherlands Balkema A. A., vol. 1, 1983.

3 M. J. M. Wagner, B. Dittrich-Hannen, H. A. Synal, M. Suter and U. Schotterer, *Nuc. Instr. Meth. Phys. Res. B*, 1996, **113**, 490–494.

4 H. Reithmeier, V. Lazarev, W. Rühm, M. Schwikowski, H. W. Gäggeler and E. Nolte, *Env. Sci. Tech.*, 2006, **40**, 5891-5896.

5 H. Reithmeier, V. Lazarev, W. Rühm and E. Nolte, *Science Tot. Env.*, 2010, **408**, 5052–5064.

6 A. Aldahan, V. Alfimov and G. Possnert, *App. Geochem.*, 2007, **22**, 606–618.

7 E. Englund, A. Aldahan, X. L. Hou, G. Possnert and C. Söderström, *Nuc. Instr. Meth. Phys. Res. B*, 2010, **268**, 1139–1141.

8 B. Sinnott, E. Ron and A. B. Schneider, *Endoc. Rev.*, 2010, **31**, 756–773.

9 R. Michel, E. Daraoui, M. Gorny, D. Jakob, R. Sachse, L. Tosch, H. Nies, I. Goroncy, J. Herrmann, H. -A. Synal, M. Stocker and V. Alfimov, *Sci. Tot. Env.*, 2012, **419**, 151-169.

10 P. H. Santschi, C. Xu, S. Zhang, Y. Ho, H. Li, K. Schwehr and D. I. Kaplan, *Technical report SRNL-STI*, 2012, 00592.

606 11 P. He, X. Hou, A. Aldahan and G. Possnert, *J. Radioanal. Nucl. Chem.*, 2014, **299**, 249-
607 253.

608 12 X. Chen, M. Gong, P. Yi, A. Aldahan, Z. Yu, G. Possnert and L. Chen, *Nuc. Inst. Meth.*
609 *Phys. Res. B*, 2015, **361**, 604–608.

610 13 G. Audi, F. G. Kondev, M. Wang, W. J. Huang and S. Naimi, *Chinese Phys. C*, 2017, **41**,
611 1–138.

612 14 A. Goel, J. S. McCloy, R. Pokorny and A. A. Kruger, *J. Non-Cryst. Solids: X*, 2019, **4**,
613 100033.

614 15 L. Campayo, A. Grandjean, A. Coulon, R. Delorme, D. Vantelon and D. Laurencin, *J.*
615 *Mat. Chem.*, 2011, **21**, 17609.

616 16 L. Campayo, S. Le Gallet, D. Perret, E. Courtois, C. Cau Dit Coumes, Y. Grin and F.
617 Bernard, *J. Nuc. Mat.*, 2015, **457**, 63–71.

618 17 E. Maddrell, A. Gandy and M. Stennett, *J. Nuc. Mat.*, 2014, **449**, 168–172.

619 18 E. R. Maddrell, E. R., Vance, C. Grant, Z. Aly, A. Stopic, T. Palmer, J. Harrison and D. J.
620 Gregg, *J. Nuc. Mat.*, 2019, **517**, 71-79.

621 19 B. J. Riley, J. D. Vienna, D. M. Strachan, J. S. McCloy and J. L. Jr. Jerden, *J. Nuc. Mat.*,
622 2016 **470**, 307-326.

623 20 A. Coulon, A. Grandjean, D. Laurencin, P. Jollivet, S. Rossignol and L. Campayo, *J. Nuc.*
624 *Mat.*, 2017, **484**, 324–331.

625 21 A. -L. Chabauty, L. Campayo, F. O. Méar and L. Montagne, *J. Non-Cryst. Solids*, 2019,
626 **510**, 51-61.

627 22 K. Yang, W. Zhu, S. Scott, Y. Wang, J. Wang, B. J. Riley, J. Vienna and J. Lian, *J.*
628 *Hazard. Mater.*, 2021, **401**, 123279.

629 23 I. W. Donald, B. L. Metcalfe and R. N. J. Taylor, *J. Mat. Science*, 1997, **32**, 5851-5887.

630 24 A. Grandjean, M. Malki, V. Montouillout, F. Debruycker and D. Massiot, *J. Non-Cryst.*
631 *Solids*, 2008, **354**, 1664-1670.

632 25 M. I. Ojovan and W. E. Lee, *Met. Mat. Trans. A*, 2011, **42**, 837-851.

633 26 S. Gin, X. Beaudoux, F. Angéli, C. Jégou and N. Godon, *J. Non-Cryst. Solids*, 2012, **358**,
634 2559–2570.

635 27 S. Gin, P. Jollivet, M. Tribet, S. Peuget and S. Schuller, *Radiochim. Acta*, 2017, **105**, 927–
636 959.

637 28 S. Peuget, E. A. Maugeri, T. Charpentier, C. Mendoza, M. Moskura, T. Fares, O. Bouty
638 and C. Jégou, *J. Non-Cryst. Solids*, 2013, **378**, 301-312.

639 29 M. Collin, M. Fournier, P. Frugier, T. Charpentier, M. Moskura, L. Deng, M. Ren, J. Du
640 and S. Gin, *Nature Mat. Degrad.*, 2018, **2**, 1-12.

641 30 P. Hmra, *U.S. department of energy*, 2010.

642 31 I. S. Muller, D. A. McKeown and I. L. Pegg, *Proc. Mater. Sci.*, 2014, **7**, 53–59.

643 32 B. J. Riley, M. J. Schweiger, D. S. Kim, W. W. Lukens, B. D. Williams, C. Iovin, C. P.
644 Rodriguez, N. R. Overman, M. E. Bowden, D. R. Dixon, J. V. Crum, J. S. McCloy and A. A.
645 Kruger, *J. Nuc. Mat.*, 2014, **452**, 178–188.

646 33 D. A. McKeown, I. S. Muller, I. L., Pegg, *J. Nuc. Mat.*, 2015, **456**, 182–191.

34 H. Bureau, A. L. Auzende, M. Marocchi, C. Raepsaet, P. Munsch, D. Testemale, M. Mézouar, S. Kubsky, M. Carrière, A. Ricolleau and G. Fiquet, *Geochim. Cosmochim. Acta*, 2016, **173**, 114-125.

35 C. Leroy, H. Bureau, C. Sanloup, C. Raepsaet, K. Glazirin, P. Munsch, M. Harmand, G. Prouteau and H. Khodja, *Earth Planet. Science Lett.*, 2019, **522**, 144–154.

36 V. Jolivet, Y. Morizet, M. Paris and T. Suzuki-Muresan, *J. Nuc. Mat.*, 2020, **533**, 152112.

37 V. Jolivet, Y. Morizet, J. Hamon, M. Paris and T. Suzuki-Muresan, *J. Am. Cer. Soc.*, 2021, **104**, 1360-1369.

38 S. Gin, A. Abdelouas, L. J. Criscenti, W. L. Ebert, K. Ferrand, T. Geisler, M. T. Harrison, Y. Inagaki, S. Mitsui, K. T. Mueller, J. C. Marra, C. G; Pantano, E. M. Pierce, J; V. Ryan, J; M. Schofield, C. I. Steefel and J. D. Vienna, *Mater. Today*, 2013, **16**, 243–248.

39 M. R. Cicconi, E. Pili, L. Grousset, D. R. Neuville, *Mat. Res. Soc.*, 2019a, **4**, 17-18.

40 M. R. Cicconi, E. Pili, L. Grousset, P. Florian, J. C. Bouillard, D. Vantelon and D. R. Neuville, *Sci. Rep.*, 2019b, **9**, 7758.

41 Y. Morizet, M. Paris, F. Gaillard and B. Scaillet, *Geochim. Cosmochim. Acta*, 2014, **141**, 45-61.

42 Y. Morizet, N. Trcera, C. Larre, M. Rivoal, E. Le Menn, D. Vantelon and F. Gaillard, *Chem. Geol.*, 2019, **510**, 91–102.

43 J. Zhong and P. J. Bray, *J. Non-Cryst. Solids*, 1989, **111**, 67-76.

44 K. L. Ngai, Y. Wang and C. T. Moynihan, *J. Non-Cryst. Solids*, 2002, **307-310**, 999-1011.

45 S. K. Lee and J. F. Stebbins, *J. Phys. Chem B*, 2003, **107**, 3141-3148.

46 J. R. Allwardt and J. F. Stebbins, *Am. Mineral.*, 2004, **89**, 777-784.

669 47 K. E. Kelsey, J. F. Stebbins, J. L. Mosenfelder and P. D. Asimow, *Am. Mineral.*, 2009, **94**,
670 1205-1215.

671 48 J. Kjeldsen, M. M. Smedskjaer, J. C. Mauro, R. E. Youngman, L. Huang and Y. Yue, *J.*
672 *Non-Cryst. Solids*, 2013, **369**, 61–68.

673 49 S. Yueh-Ting and J. -H. Jean, *J. Am. Cer. Soc.*, 2017, **100**, 5482-5489.

674 50 M. R. Carroll and M. J. Rutherford, *J. Geophys. Res.*, 1985, **90**, 601–612.

675 51 H. S. C. O'Neill and J. A. Mavrogenes, *J. Petrol.*, 2002, **43**, 1049–1087.

676 52 B. Scaillet and M. Pichavant, *Ann. Geophys.*, 2005, **48**, 671–697.

677 53 K. Klimm, S. C. Kohn and R. E. Botcharnikov, *Chem. Geol.*, 2012, **322-323**, 250-267.

678 54 S. Ding, R. Dasgupta and K. Tsuno, *Geochim. Cosmochim. Acta*, 2014, **131**, 227-246.

679 55 Y. Morizet, R. A. Brooker and S. C. Kohn, *Geochim. Cosmochim. Acta*, 2002, **66**, 1809–
680 1820.

681 56 P. McDade, B. J. Wood, W. Van Westrenen, R. Brooker, G. Gudmundsson, H. Soulard, J.
682 Najorka and J. Blundy, *Min. Mag.*, 2002, **66**, 1021-1028.

683 57 V. Jolivet, L. Jossé, M. Rivoal, M. Paris, Y. Morizet, C. La and T. Suzuki-Muresan, *J.*
684 *Non-Cryst. Solids*, 2019, **511**, 50-61.

685 58 T. L. Barr and S. Seal, *J. Vac. Sci. Tech. A*, 1995, **13**, 1239-1246.

686 59 D. J. Miller, M. C. Biesinger and N. S. McIntyre, *Surf. Interface Anal.*, 2002, **33**, 299-305.

687 60 S. Tougaard, *Surf. Inter. Anal.*, 1997, **25**, 137-154.

688 61 T. Tojo, T. Tachikawa, M. Fujitsuka and T. Majima, *J. Phys. Chem. C*, 2008, **112**, 14948–
689 14954.

690 62 Y. Morizet, V. Jolivet, N. Trcera, T. Suzuki-Muresan and J. Hamon, *J. Nuc. Mat.*, 2021,
691 **553**, 153050.

692 63 P. Maass, *J. Non-Cryst. Solids*, 1999, **255**, 35–46.

693 64 J. Shen and D. J. Green, *J. Non-Cryst. Solids*, 2004, **344**, 66-72.

694 65 L. Cormier and G. J. Cuello, *Geochim. Cosmochim. Acta*, 2013, **122**, 498-510.

695 66 A. Marinoiu, I. Gatto, M. Raceanu, M. Varlam, C. Moise, A. Pantazi, C. Jianu, I.
696 Stefanescu and M. Enachescu, *Int. J. Hydrogen Energy*, 2017, **42**, 26877-26888.

697 67 P. Xiang, F. Lv, T. Xiao, L. Jiang, X. Tan and T. Shu, *J. Alloys Comp.*, 2018, **741**, 1142-
698 1147.

699 68 J. F. Moulder, W. F. Stickle, P. E. Sobol and K. D. Bomben, J. Chastain Ed., Perkin-Elmer
700 Corporation Physical Electronics Division, Eden Prairie, Minnesota, 1992.

701 69 K. Li, Y. Zhao, P. Zhang, C. He, C. Deng, S. Ding and W. Shi, *App. Surf. Science*, 2016,
702 **390**, 412-421.

703 70 P. M. A. Sherwood, *J. Chem. Soc., Faraday Trans. 2*, 1976, **72**, 1805-1820.

704 71 R. Kägi, *Am. Mineral.*, 2005, **90**, 708–717.

705 72 C. Larre, Y. Morizet, A. Bézos, C. Guivel, C. La and N. Mangold, *J. Raman Spec.*, 2020,
706 **51**, 493–507.

707 73 Y. Morizet, M. Paris, I. Di Carlo and B. Scaillet, *Chem. Geol.*, 2013, **358**, 131–147.

708 74 H. Zhang, T. Suzuki-Muresan, Y. Morizet, S. Gin, A. Abdelouas, *Nature Mat. Degrad.*,
709 2021, **5**, 10.

710 75 C. -C. Lin, *J. Inorg. Nucl. Chem.*, 1980, **42**, 1093-1099.

711 76 I. D. Kaplan, R. J. Serne, K. E. Parker and I. V. Kutnyakov, *Env. Sci. Tech.*, 2000, **34**, 399-
712 405.

713 77 W. Levason, *Coord. Chem. Rev.*, 1997, **161**, 33-79.

714 78 G. F. Piepel, S. K. Cooley, J. D. Vienna and J. V. Crum, U.S. department of energy,
715 Pacific Northwest National Laboratory, 2015, 24391.

716 79 W. J. Dell, P. J. Bray and S. Z. Xiao, *J. Non-Cryst. Solids*, 1983, **58**, 1-16.

717 80 L. S. Du and J. F. Stebbins, *J. Non-Cryst. Solids*, 2005, **351**, 3508–3520.

718 81 S. K. Lee and J. F. Stebbins, *Geochim. Cosmochim. Acta*, 2009, **73**, 1109-1119.

719 82 M. M. Smedskjaer, J. C. Mauro, R. E. Youngman, C. L. Hogue, M. Potuzak and Y. Yue, *J.*
720 *Phys. Chem. B*, 2011, **115**, 12930–12946.

721 83 J. F. Stebbins, *Am. Mineral.*, 2016, **101**, 753–768.

722 84 A. Quintas, D. Caurant, O. Majérus, T. Charpentier and J. -L. Dussossoy, *Mater. Res.*
723 *Bull.*, 2009, **44**, 1895-1898.

724 85 E. Gambuzzi, T. Charpentier, M. C. Menziani and A. Pedone, *Chem. Phys. Letters*, 2014,
725 **612**, 56–61.

726

727 **Figure caption**

728 Figure 1: I concentration measured by LA-ICP-MS as a function of I concentration measured
729 by SEM EDS. The 1:1 line is reported. The provided error is calculated from the standard
730 deviation of the replicated measurements: at least 5 spots by LA-ICP-MS, 10 scans by SEM
731 EDS.

Figure 2: I concentration determined by LA-ICP-MS for $C_{20}N_{15}$-22 glass sample. The I content was measured along and across the Pt capsule to determine the homogeneity with respect to I content. 48 spots were acquired through the entire experimental charge. The average I concentration is 4.6 mol.% and the standard deviation is ±0.1 mol.%.

Figure 3: Change in I solubility as a function of XNa = Na/(Na+Ca) for the investigated glasses. The I solubility for the three experimental series is represented: CN-I_2 (CN-1), CN-I_2O_5 (CN-2) and CN-I_2O_5+PtO_2 (CN-3). I solubility can reach up to 5.7 mol.% and is maximised for CN-2 glass series in which I is dissolved as I^{5+}.

Figure 4: XPS spectra obtained for $C_{35}N_0$ and C_0N_{35} glasses showing I dissolved mainly as I^- (CN-1) or I^{5+} (CN-2). The spectrum simulations are also reported along with the quantified species. We show that I dissolves as several species in the glasses: I^- (~610 eV) and I^0 (~621 eV) for the less oxidized ones (CN-1); I^{5+} (~624 eV), I^- and I^0 for the most oxidized ones (CN-2).

Figure 5: Distribution of I speciation as measured by XPS on four glass chips for $C_{35}N_0$-2 glass. The I speciation appears relatively homogeneous in $C_{35}N_0$-2 glass (±10%).

Figure 6: XPS spectra obtained on $C_{35}N_0$-33 showing the presence of I^{7+} species (~626 eV) along with I^{5+}, I^- and I^0 species dissolved in the glass. Spectra are shown for several cycles of acquisitions. There is a gradual decrease in the I^{7+} concentration from 30.3 to 3.8% between Cycles 1 and 9, respectively; demonstrating the weak stability of I^{7+} within the glass under the X-ray beam. The entire set of data is provided in the Suppl. Mat..

Figure 7: Change in the I species concentrations (I^{7+}, I^{5+}, I^-, I^0) as a function of the XPS cycle for $C_{35}N_0$-33. Periodate I^{7+} is gradually converted to iodate I^{5+}; and I^{7+} concentration is close to 0 after 10 XPS cycles.

Figure 8: I solubility as a function of the I Overall Redox State (ORS). The ORS is calculated from Eq. 1 and using the I speciation obtained from XPS spectrum simulations. An estimate of the fO_2 conditions is provided: QFM+1 in CN-1 series and QFM+3 in CN-2 series. The I solubility is positively correlated to the increase in oxidizing conditions for Na-bearing glass compositions (i.e. from $C_{30}N_5$ to C_0N_{35}) but seems unaffected for Ca-bearing glass (i.e. $C_{35}N_0$).

762

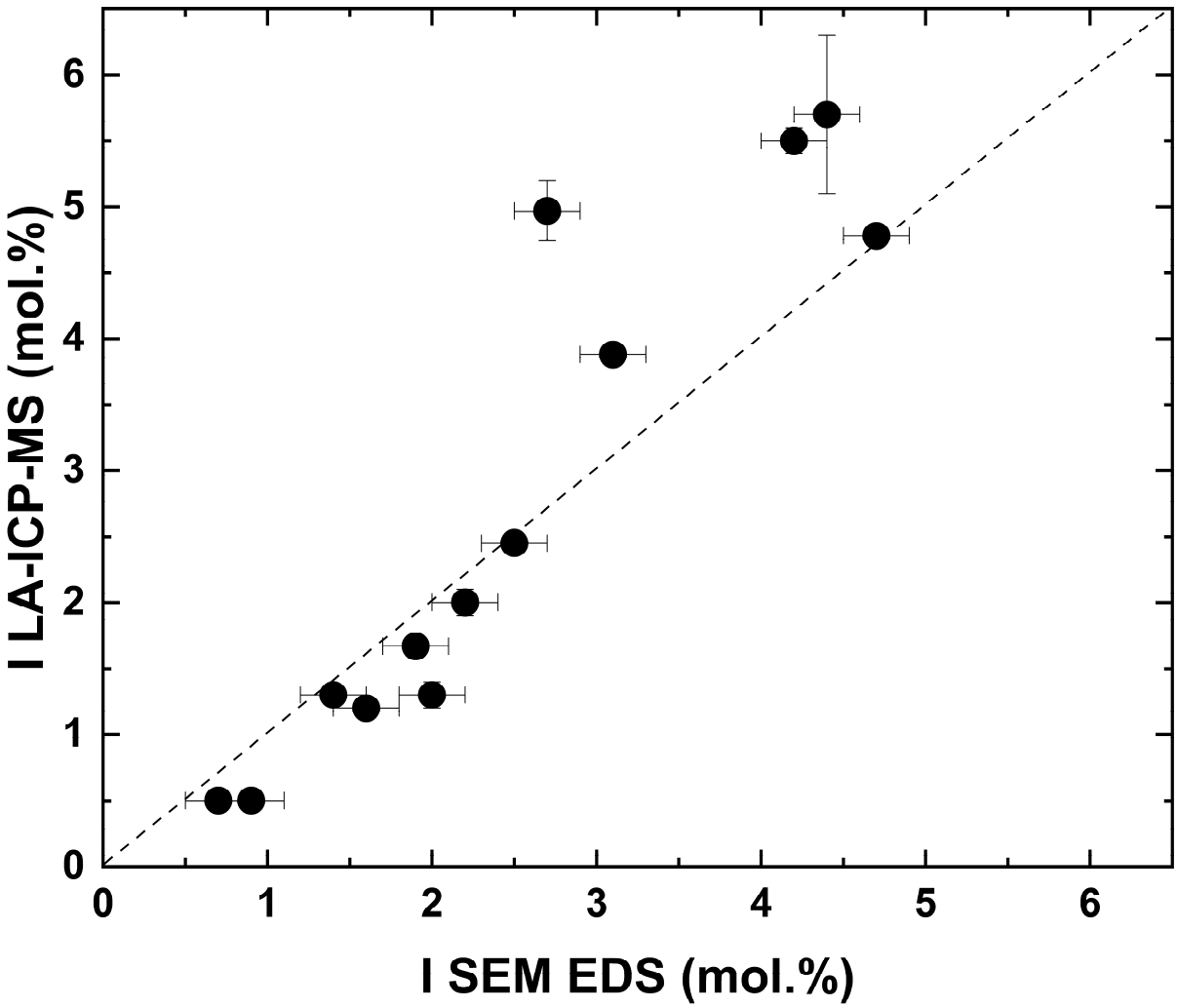

763

764 Figure 1

765

766

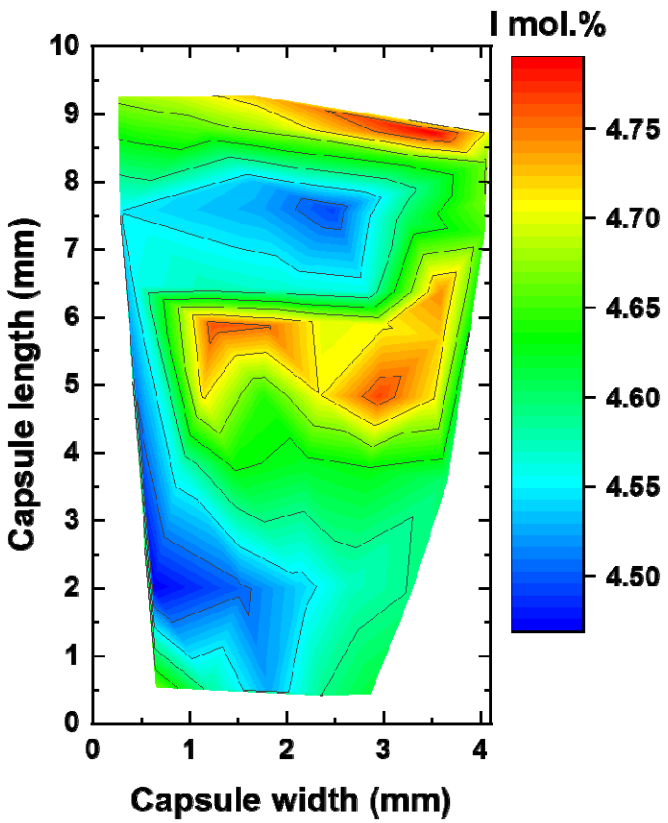

767

768 Figure 2

769

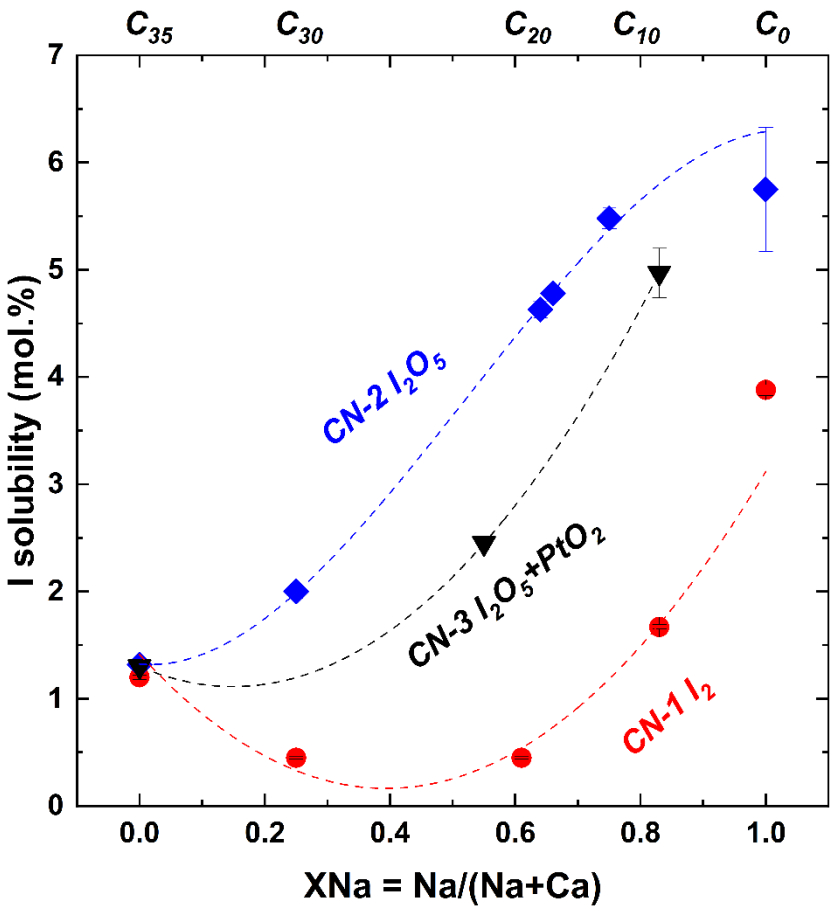
C35
C30
C20
C10
C0
I solubility (mol.%)
XNa = Na/(Na+Ca)
CN-2 I2O5
CN-3 I2O5+PtO2
CN-1 I2
0
1
2
3
4
5
6
7
0.0
0.2
0.4
0.6
0.8
1.0

Figure 3

774

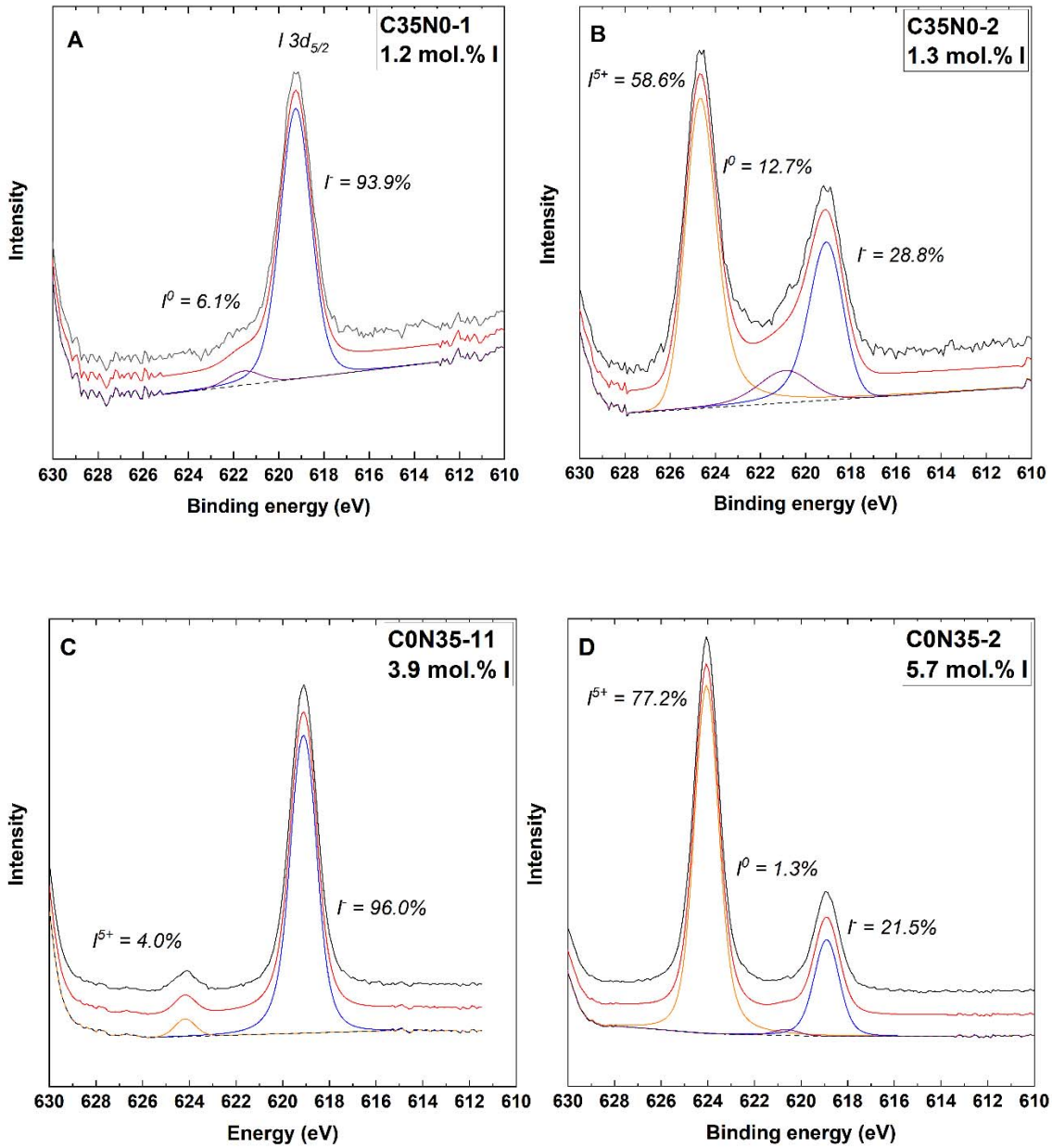

775

776

777 Figure 4

778

779

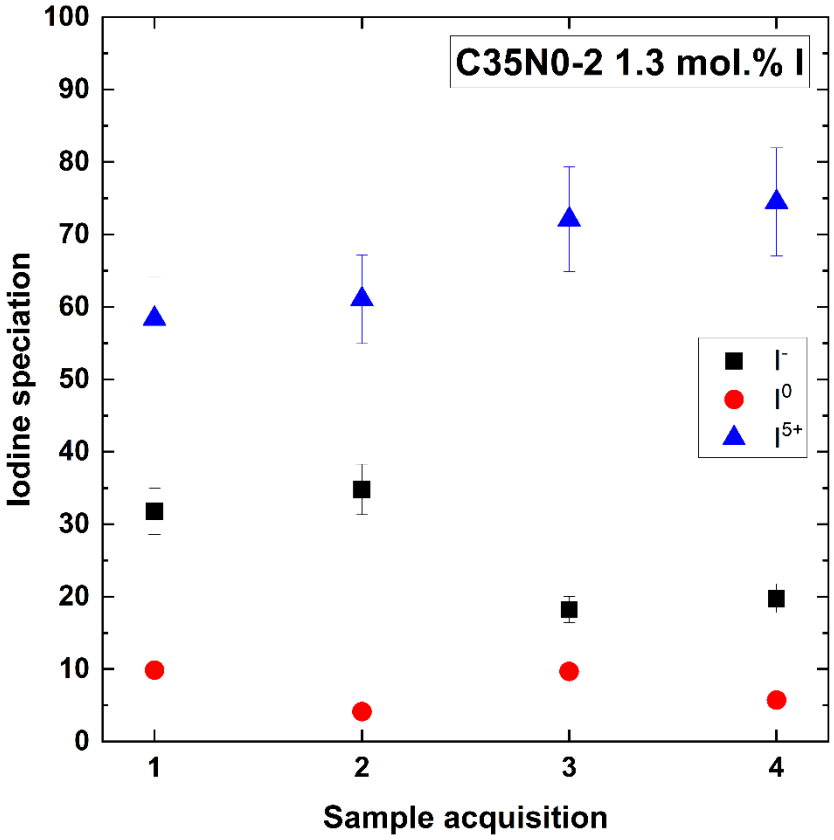

780

781 Figure 5

782

783

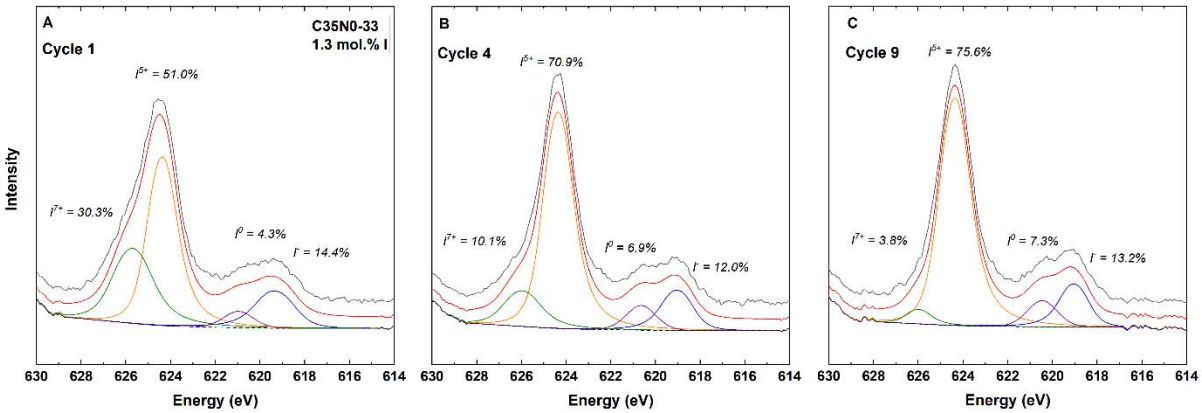

784

785 Figure 6

786

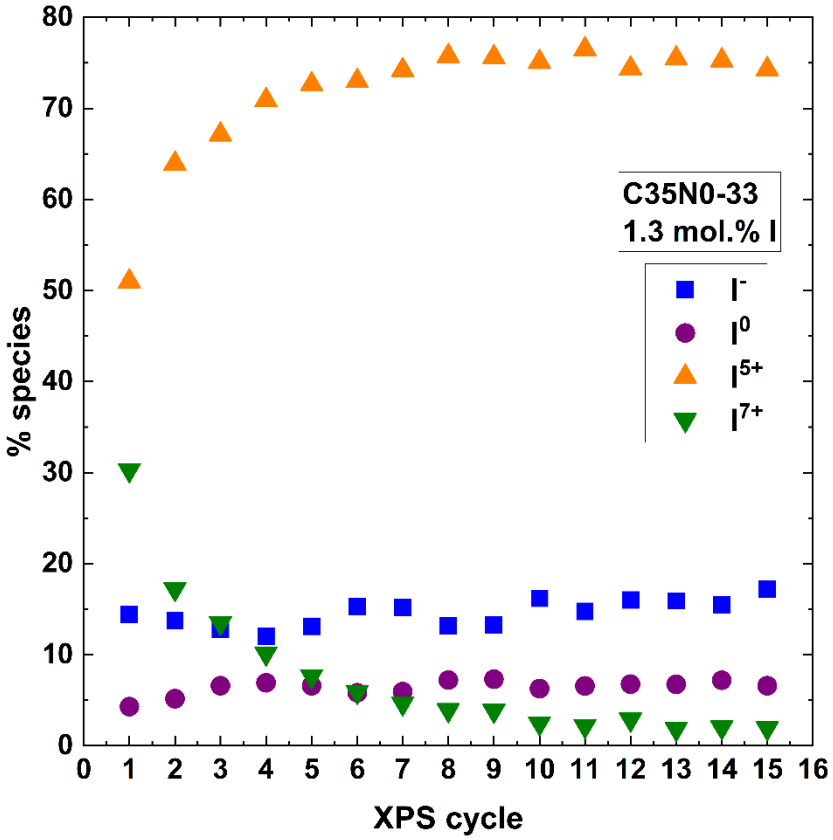
C35N0-33
1.3 mol.% I
I-
I0
I5+
I7+
% species
XPS cycle
0
10
20
30
40
50
60
70
80
0 1 2 3 4 5 6 7 8 9 10 11 12 13 14 15 16

Figure 7

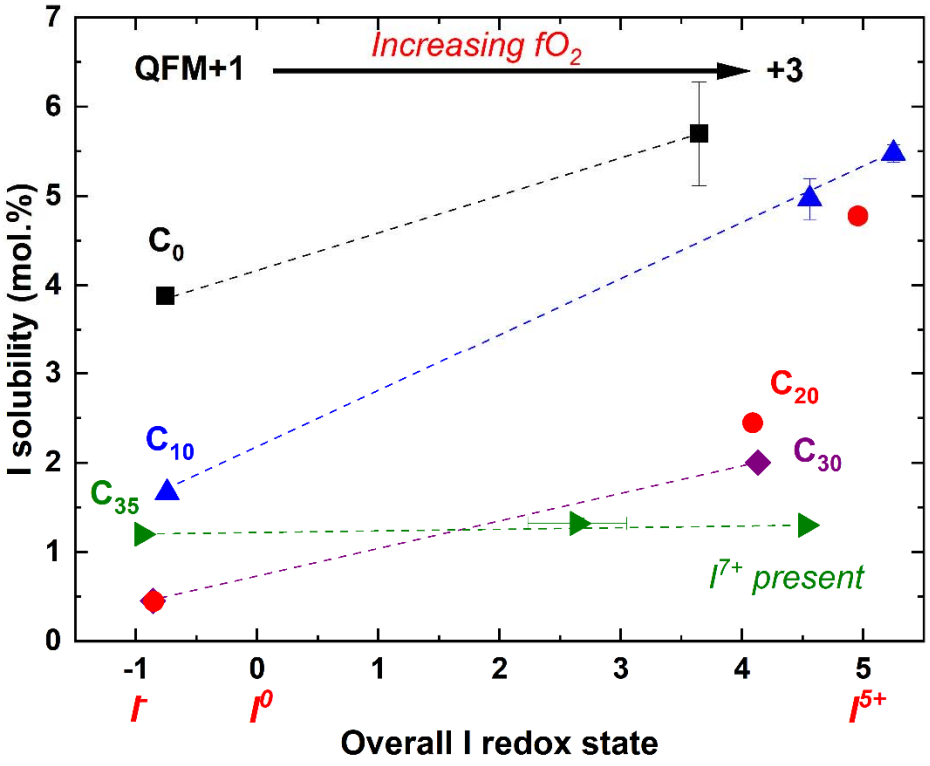
QFM+1
Increasing fO_2
+3
C_0
C_{10}
C_{20}
C_{30}
C_{35}
I^{7+} present
I solubility (mol.%)
Overall I redox state
I^-
I^0
I^{5+}

Figure 8

Table 1: Major elements, I solubility and speciation for CN glass series loaded with I_2 (CN-1), I_2O_5 (CN-2) and I_2O_5+PtO_2 (CN-3).

Sample	I loaded (mol.%)	Added O_2 (mol.%)	Major elements (mol.%)[a]						I speciation[b]					I solubility (mol.%)[d]	
			SiO_2	B_2O_3	Al_2O_3	CaO	Na_2O	XNa	I^-	I^0	I^{5+}	I^{7+}	I Overall Redox State (ORS)[c]	I SEM EDS	I LA ICP MS
CN-0 I-free 0.0001 GPa 1200°C															
$C_{35}N_0$-0	0	0	32.4	29.1	4.9	33.6	0	0							
$C_{30}N_5$-0	0	0	31.7	29.7	5.2	28.4	5.0	0.26							
$C_{20}N_{15}$-0	0	0	33.9	29.0	5.0	17.9	14.3	0.62							
$C_{10}N_{25}$-0	0	0	32.9	29.6	4.9	8.9	23.6	0.84							
C_0N_{35}-0	0	0	31.5	30.7	5.3	0	32.5	1							
CN-1 I_2 loaded 1.5 GPa 1400°C 4h															
$C_{35}N_0$-1	13.4	0	31.8	29.2	4.9	32.5	0	0	93.9	6.1	0		-0.94	1.6	1.2
$C_{30}N_5$-1	13.3	0	32.1	29.9	5.0	27.7	4.7	0.25	86.4	13.6	0		-0.86	0.7	0.5
$C_{20}N_{15}$-1	12.9	0	33.5	30.0	4.8	17.4	13.4	0.61	94.1	5.9	0		-0.94	0.9	0.5
$C_{10}N_{25}$-1	13.5	0	31.6	31.1	5.1	8.8	21.5	0.83	85.2	14.8	0		-0.85	1.9	1.7
C_0N_{35}-11	12.4	0	31.5	29.2	5.3	0	31.0	1	96.0	0	4.0		-0.76	3.1	3.9
CN-2 I_2O_5 loaded 1.5 GPa 1400°C 4h															
$C_{35}N_0$-2	12.6	15.7	32.0	23.8	5.2	36.9	0	0	28.8	12.7	58.6		2.64	2.0	1.3
$C_{30}N_5$-2	13.1	16.4	31.2	27.3	5.2	29.3	4.8	0.25	14.5	0	85.5		4.13	2.2	2.0
$C_{20}N_{15}$-2	12.6	15.8	31.6	26.9	5.1	15.3	14.9	0.66	9.2	8.2	82.5		4.03	4.7	4.8
$C_{20}N_{15}$-22[e]	12.1	16.2	32.0	28.6	4.8	16.1	14.1	0.64	nd	nd	nd		nd	4.4	4.6
$C_{10}N_{25}$-2	12.9	16.7	31.6	28.4	5.4	11.5	17.5	0.75	9.9	2.4	87.7		4.29	4.2	5.5
C_0N_{35}-2	13.4	15.1	31.6	29.9	5.3	0	28.9	1	21.5	1.3	77.2		3.65	4.4	5.7
CN-3 I_2O_5 + PtO_2 loaded 1.5 GPa 1400°C 4h															
$C_{35}N_0$-33	12.0	18.8	33.0	29.8	5.6	30.3	0	0	14.5	4.3	51.0	30.3	4.53	1.4	1.3
$C_{20}N_{15}$-3	13.1	20.4	34.8	29.5	5.8	17.0	10.5	0.55	28.5	0	71.5		3.29	2.5	2.5
$C_{10}N_{25}$-3	13.6	21.6	33.0	29.8	5.7	8.3	20.9	0.83	21.8	0	78.2		3.69	2.7	5.0

[a]The major element concentrations are determined by SEM EDS, the ISG (Gin et al. 2013) was used as a chemical reference.

[b]The I speciation is determined from the simulation of the XPS spectra acquired in the I 3d spectral region (610-640 eV). The error on each species concentration is estimated to be better than 10% in relative to the value.

[c]The I Overall Redox State represents an empirical value corresponding to the balance between the different oxidation states (I^-, I^0, I^{5+}) determined through the XPS analysis.

[d]The I content is measured in the bulk glass. The error bar obtained on each value is obtained on the replicated analyses. Typical error on the SEM EDS measurement is ±0.2 mol.% and the typical error on the LA ICP MS measurement is better than 0.1 mol.%.

[e]The C20N15-22 is a solid copy of the C20N15-2, to assess the reproducibility of the method. The I solubility has been measured by LA ICP MS with the acquisition of 48 analytical points.